Rare Metal Materials and Engineering
Volume 51, Issue 1, January 2022
Available online at www.rmme.ac.cn

Science Press

Cite this article as: Huang Zhen, Yuan Wuhua, Zhu Jiajia. Low Temperature Stress Relaxation and Morphology Evolution of Ti-6.5Al-2Zr-1Mo-1V Titanium Alloys[J]. Rare Metal Materials and Engineering, 2022, 51(01): 83-91.

ARTICLE

Low Temperature Stress Relaxation and Morphology Evolution of Ti-6.5Al-2Zr-1Mo-1V Titanium Alloys

Huang Zhen, Yuan Wuhua, Zhu Jiajia

College of Materials Science and Engineering, Hunan University, Changsha 410082, China

Abstract: Stress relaxation tests were performed on Ti-6.5Al-2Zr-1Mo-1V titanium alloys with different initial stresses at 500, 550, and 600 °C. Based on the classical Maxwell exponential decay function, the stress relaxation limit was obtained. The relaxation stability coefficient (C_S) and relaxation rate coefficient (C_R) were proposed to describe the relaxation characteristics and to further guide the residual stress reduction. The stress exponent was calculated according to Norton and Arrhenius equations. Both the stress exponent and microstructure were analyzed to illustrate the stress relaxation mechanism. Under different initial stresses, the dislocation climb and diffusion dominate the stress relaxation procedure at 500 °C; the dislocation slip plays a major role in stress relaxation at 550 °C; the dislocation slip, boundary slip, and grain rotation control the stress relaxation process at 600 °C.

Key words: titanium alloys; stress relaxation; microstructure; relaxation mechanism

The titanium alloys with high strength, low density, and excellent corrosion resistance are widely used in the aerospace industry as beam rib and bulkhead in craft[1-3]. The Ti-6.5Al-2Zr-1Mo-1V titanium alloy with excellent high temperature performance becomes one of the most important candidates for aerospace structural parts[4]. However, the residual stress generated in the formation process and heat treatment of titanium alloy seriously affects its performance[5]. Hrabe[6] and Baragetti[7] et al studied the effect of residual stress on the fatigue properties of Ti6-Al4-V alloys fabricated via electron beam melting under different stress gradients, and found that the existence and distribution of stress severely affect the fatigue life of titanium alloys.

The essence of stress relaxation is that the internal elastic strain is gradually converted into plastic strain when the metal material is deformed[8]. In the last several decades, the stress relaxation tests (SRTs) have been performed to obtain the stress relaxation curves and the creep-type stress relaxation constitutive equations of titanium alloys at the service temperature. Dupeux et al[9] proposed an empirical hyperbolic law of stress relaxation, and Liu et al[10] proposed the stress-time curve to describe the stress relaxation curves. There are many methods to describe the stress relaxation, and how to obtain the relaxation mechanism from stress relaxation curves is the key problem. Zong et al[11] investigated the high temperature short-term creep and the stress relaxation of Ti6-Al4-V alloys. The stress exponent of 1.52~1.97 at 973 K and 1.60~1.69 at 1023 K is calculated to reflect the relaxation or creep mechanism under different temperatures and stresses. Luo et al[12] studied the effect of different grain sizes on the stress relaxation mechanism. The stress exponent of 1.260~2.144 can be obtained with different grain sizes. For the alloys with coarse grains, the dislocation movement, including the dislocation slip and dislocation climb, dynamic recovery, and recrystallization can dominate the stress relaxation process. The combining effects of grain rotation, grain boundary slip, and dislocation movement are the major mechanisms for alloys with fine grains. Zhu et al[13] studied the stress-strain rate relationship obtained from SRTs of Al-Mg alloys. To predict the relaxation damage life of bolting material 1Cr10NiMoW2VNbN, Guo et al[14] proposed a SRT damage model in accordance with related creep data.

Most research focuses on the stress relaxation model, the effect of grain size on stress relaxation, and the relationship between stress relaxation and creep at high temperature to estimate the high-temperature properties and service life evaluation[15-18]. The effect of annealing temperature on stress relaxation behavior of titanium alloys was rarely reported. In

Received date: January 14, 2021
Corresponding author: Yuan Wuhua, Ph. D., Professor, College of Materials Science and Engineering, Hunan University, Changsha 410082, P. R. China, E-mail: yuan731115@hnu.edu.cn

the process of reducing the residual stress by heat treatment, the process temperature (773~873 K) is much lower than the deformation temperature (1213~1273 K). Besides, due to lower elastic modulus, the large-scale parts of titanium alloy are prone to deform due to the release of residual stress. Therefore, it is necessary to control the residual stress for high dimensional accuracy of parts[19]. The theoretically basic condition of residual stress release is the long-term stress relaxation at low temperature[20]. During the stress relaxation, the higher temperature of 0.4~0.6 times as large as the melting temperature T_m instead of 0.3 times as large as T_m is commonly considered. Therefore, the short-term stress relaxation behavior of Ti-6.5Al-2Zr-1Mo-1V titanium alloys at low temperature should be investigated to determine the process parameters for reducing the residual stress.

In this research, SRTs of Ti-6.5Al-2Zr-1Mo-1V titanium alloys were performed with different initial stresses at different temperatures. Based on the stress relaxation curves, the relaxation amplitude, relaxation stability, and relaxation rate coefficient were obtained. The stress exponent was calculated to reflect the relaxation mechanism of titanium alloys under different temperatures and different initial stresses.

1 Experiment

The Ti-6.5Al-2Zr-1Mo-1V titanium alloys were treated by hot forging and annealing at 850 °C for 3 h. The length and width of specimens was 185 and 10 mm, respectively. SRTs were conducted through an electronic creep testing machine. An extensometer with the accuracy of 0.5% was used for elongation measurement. A closed-loop controlled system was used to maintain the constant loading or strain. Besides, a three-zone fired furnace was used to provide an isothermal environment. During the test, three thermocouples were attached to the top, middle, and bottom sections of specimen surface in the purpose of accurate temperature monitoring. The tests were conducted at temperatures of 500, 550, and 600 °C for 10 h under the initial stress of 100, 200, and 300 MPa. After SRTs, the deformed specimens were cooled inside the furnace. The specimens for metallographic observation were cut off from the middle section of specimens and observed by optical microscope (OM). The crystallographic characteristics of the specimens were characterized by mini-Flex X-ray diffractometer (XRD) with Cu-Kα (λ=0.154 05 nm) radiation source operated at 45 kV and 40 mA. The thin foils for transmission electron microscope (TEM) and electron back scattering diffraction (EBSD) analyses were prepared by mechanical polishing and twin jet electrolytic polishing methods.

2 Result and Discussion

2.1 Stress relaxation curves

Fig. 1 shows the stress-relaxation time curves of Ti-6.5Al-2Zr-1Mo-1V titanium alloys at different temperatures and initial stresses. The stress relaxation process can be divided into two periods. The stress is decreased swiftly with increasing the relaxation time at first, because of a large amount of dislocation slip. Then the stress decreases gently towards a certain constant. It can be seen that the higher the temperature, the lower the stress relaxation limit (SRL) under the same initial stress. Besides, it can be concluded that SRL at the same temperature under different initial stresses tends to be similar with infinitely extending the relaxation time.

2.1.1 Stress relaxation behavior

The slowly decreasing period of stress should be deeply investigated because heat treatment is a long-term process. The stress relaxation amplitude (σ_∞/σ_0), relaxation stability coefficient (C_S), and relaxation rate coefficient (C_R) are used to describe the magnitude, tendency, and speed of stress relaxation, respectively. SRL can be calculated by Maxwell equation based on exponent decay, as shown in Fig. 1. The relaxation stability coefficient and relaxation rate coefficient can be calculated by Eq.(1) and Eq.(2), respectively, as follows:

$$C_S=\sigma/\sigma_0 \quad (1)$$

$$C_R=1/K \quad (2)$$

where σ_0 is the initial stress; σ and K are the intercept and slope of the fitting line of stress relaxation curves in slowly decreasing period, respectively.

Fig.2a shows the stress relaxation amplitude under different conditions. When the relaxation temperature reaches 500 °C, the stress relaxation amplitude is 64.44%, 57.58%, and 54.89% with the initial stress of 100, 200, and 300 MPa,

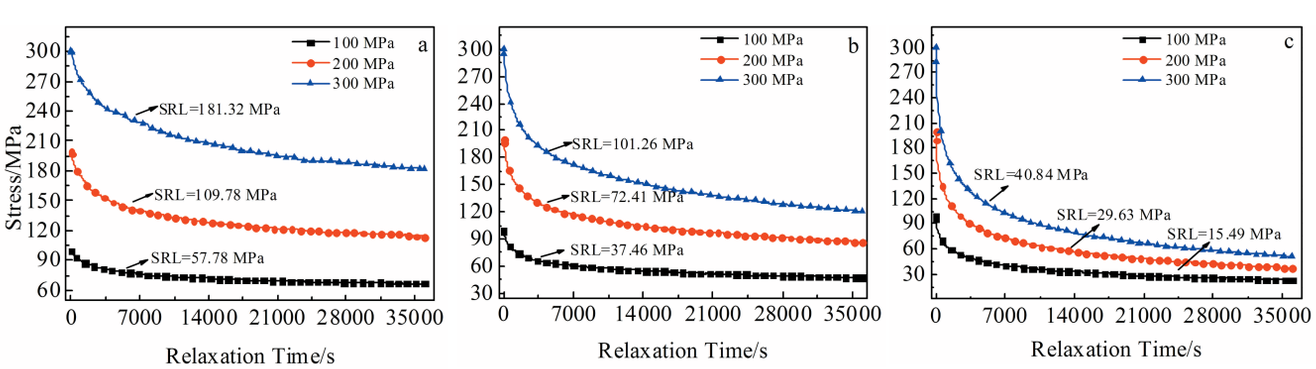

Fig.1 Stress relaxation curves of specimens under different initial stresses at 500 °C (a), 550 °C (b), and 600 °C (c)

respectively, indicating that the higher the initial stress, the greater the stress relaxation. However, the stress relaxation amplitude changes slightly at 600 °C, which is 15.49%, 14.81%, and 13.61% with the initial stress of 100, 200, and 300 MPa, respectively. This result suggests that better enhancement effect of residual stress reduction is hard to achieve after the temperature and initial stress reach the threshold value. According to Fig. 2b, because higher C_S represents greater stress relaxation resistance, the relaxation stability is mainly determined by temperature rather than the initial stress, and it decreases rapidly at 600 °C compared with that at 500 °C. According to Fig.2c, C_R is determined by both the temperature and initial stress, and it is decreased obviously with increasing the initial stress from 100 MPa to 300 MPa at the same temperature. However, C_R hardly changes as the temperature increases from 500 °C to 600 °C under the initial stress of 300 MPa. In general, the small stress reduction can be achieved at 600 °C, whereas under the condition of high stress, the stress relaxation temperature of 500 °C is a better choice.

2.1.2 Stress exponent

In the entire stress relaxation process, the total strain (ε_0) is a constant, but the elastic strain (ε_e) is gradually transformed into plastic strain (ε_p), as expressed by Eq.(3), as follows:

$$\varepsilon_0=\varepsilon_e+\varepsilon_p \tag{3}$$

Considering the elastic Hooke's law, Eq. (1) can be transformed into Eq.(4)[16], as follows:

$$\dot{\varepsilon}_{SR}=-\frac{1}{E}\frac{d\sigma}{dt} \tag{4}$$

where $\dot{\varepsilon}_{SR}$ is the strain rate from stress relaxation, E denotes the elastic modulus, and t is the relaxation time. Therefore, the stress relaxation can be described by Norton equation, as follows:

$$\dot{\varepsilon}_{SR}=A_1\sigma^{n_{SR}} \tag{5}$$

where A_1 is a material-dependent constant and n_{SR} is the stress exponent. Thus, the stress relaxation is a thermally-activated process, which can be described by Arrhenius equation, as follows:

$$\dot{\varepsilon}_{SR}=A_2\exp\left(-\frac{Q_{SR}}{RT}\right) \tag{6}$$

Combining Eq. (3) and Eq. (4), $\dot{\varepsilon}_{SR}$ can be expressed by Eq.(7), as follows:

$$\dot{\varepsilon}_{SR}=A\sigma^{n_{SR}}\exp\left(-\frac{Q_{SR}}{RT}\right) \tag{7}$$

where, A is a constant related to A_1 and A_2. In order to obtain the stress exponent, take the natural logarithm on both sides of Eq.(7):

$$\ln\dot{\varepsilon}_{SR}=\ln A+n_{SR}\ln\sigma-\frac{Q}{RT} \tag{8}$$

Fig. 3 reveals the curves of steady strain rate-stress from

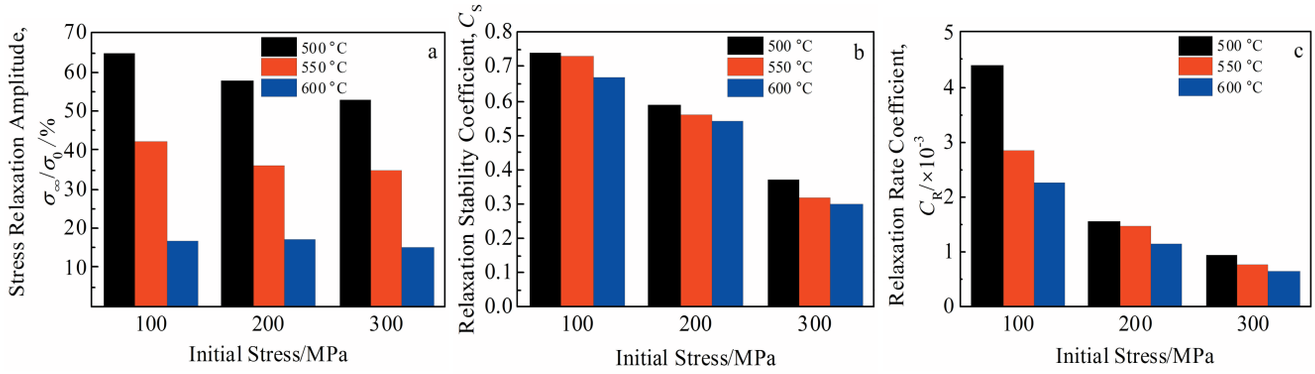

Fig.2 Stress relaxation amplitude (a), relaxation stability coefficient (b), and relaxation rate coefficient (c) of specimens under different initial stresses at different temperatures

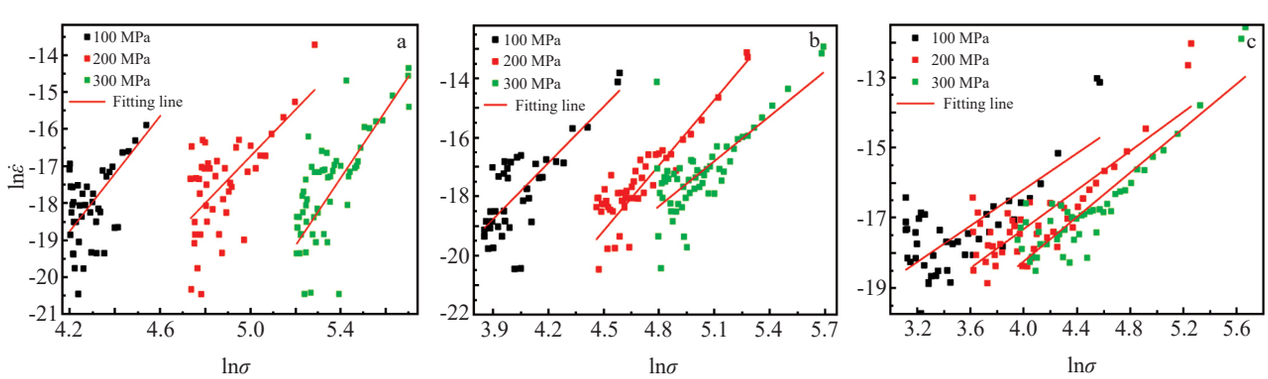

Fig.3 Relationship of lnε̇-lnσ of specimens under different initial stresses at 500 °C (a), 550 °C (b), and 600 °C (c)

SRTs. The stress exponent under different temperatures and initial stresses can be determined by the gradient of $\ln\dot{\varepsilon}/\ln\sigma$, and the results are shown in Table 1. In general, the stress exponent is 2.38~7.76. At 500 °C, the stress exponent is 5.97~7.76, indicating that the dislocation climb dominates the stress relaxation process, although the dislocation slip also plays an important role. With increasing the initial stress and temperature, the stress exponent becomes smaller, suggesting that the slip system becomes easier to start and more dislocation slips participate in this procedure. The main mechanism is the dislocation slip when the stress exponent is about 3. At 600 °C, the stress exponent is less than 3 and gradually decreased with increasing the initial stress, indicating that the grain boundary slip controls the stress relaxation. Thus, the effect of the boundary slip is more obvious with increasing the initial stress.

2.2 Stress relaxation mechanism

Fig. 4 shows XRD patterns of original titanium alloy and specimens after stress relaxation under different conditions. Compared with the annealed alloy, the (101), (002), (101) peaks are shifted in different extents after stress relaxation, indicating the lattice distortion on different crystal planes. The larger the residual stress after stress relaxation, the greater the degree of left deviation. After stress relaxation, the intensity of some α phase peaks weakens, and the peak of β phase occurs. This phenomenon reflects that the phase transformation occurs after stress relaxation. In addition, EBSD measurement shows that the content of β phase is 1.99%, 3.23%, 3.31%, 5.32%, and 12.8% in the annealed alloy and the specimens after stress relaxation under 100 MPa at 500 °C, under 300 MPa at 500 °C, under 100 MPa at 600 °C, and under 300 MPa at 600 °C, respectively.

Table 1 Stress exponents of specimens under different initial stresses and different temperatures

Initial stress/MPa	Temperature/°C		
	500	550	600
100	7.76	5.51	2.75
200	6.31	4.01	2.47
300	5.97	3.98	2.38

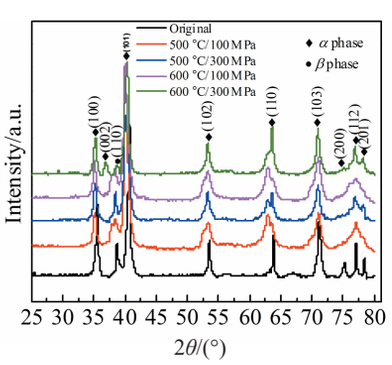

Fig.4 XRD patterns of original alloy and specimens under different initial stresses and different temperatures

Fig. 5 shows EBSD grain boundary orientation distributions of the original alloy and the specimens after stress relaxation at 500 and 600 °C under initial stress of 100 and 300 MPa. It can be seen that the low angle grain boundary (LAGB, 2°~15°) exists in some grains, which is formed after α+β forging and annealing, and LAGBs account for 18.3% of entire area in Fig. 5a. However, after the stress relaxation under initial stress of 100 MPa at 500 °C, the fraction of LAGBs changes slightly to 16.7%, which means that dislocation slip creep hardly happens. TEM images of original alloy and the one after stress relaxation under initial stress of 100 MPa at 500 °C are shown in Fig. 6a and 6b, respectively. In the original annealed specimen, a few dislocations can be observed in α grains, which are generated after forging and annealing. There are many short and parallel dislocation lines after stress relaxation under initial stress of 100 MPa. Meanwhile, β transformation structure can be observed between α grains. It can be found that there are many α/β interfaces. Thus, the dislocation is difficult to pass through by slipping and enter the next grain. But the numerous phase interfaces indicate that there are many channels for atom diffusion. So the dislocation climb controlled by diffusion occurs more easily. Therefore, the dislocations are firstly rearranged by slip and then controlled by climbing into the α grain. When the dislocation density reaches a certain value, the dislocation cells gradually change into sub-grain boundaries and generate sub-grains. The fraction of LAGBs increases to 25.6% as the initial stress increases to 300 MPa, which illustrates that the recovery creep happens and the dislocation slip plays an important role. With increasing the initial stress, more edge dislocations begin to participate in the dislocation slip, as shown in Fig. 5c. When the dislocations are stacked, the dislocation slip is hindered and the dislocations are entangled to generate sub-grain boundary. Meanwhile, the stress relaxation temperature is approximately equal to $0.3T_m$ and the α/β interface is still an obstacle. Therefore, the edge dislocation climb also controls the stress relaxation process. However, the fraction of LAGBs increases to 32.8% under initial stress of 100 MPa at 600 °C. A large number of sub-grains are generated, indicating that the dynamic recovery effect is significant and the cross slip of screw dislocation can release the stress gradually. Fig. 6d shows TEM image of specimen under initial stress of 100 MPa at 600 °C. The dislocation entanglement appears in α grains. Meanwhile, a small amount of β phase appears between α grains, providing favorable conditions for the rotation of α grains. But the grains with size of 14~18 μm increase substantially. The grain growth is closely related to the atom diffusion behavior and grain boundary migration. Fig. 5e shows that the fraction of LAGBs is 65.1%. This result implies that abundant sub-grain boundaries are generated when the initial stress changes to 300 MPa and more screw dislocations participate in the stress relaxation process. Thus, it can be seen that many small grains with polygonization shape are generated. In addition, the fraction of β phase increases to 12%, indicating that the number of α/β interfaces

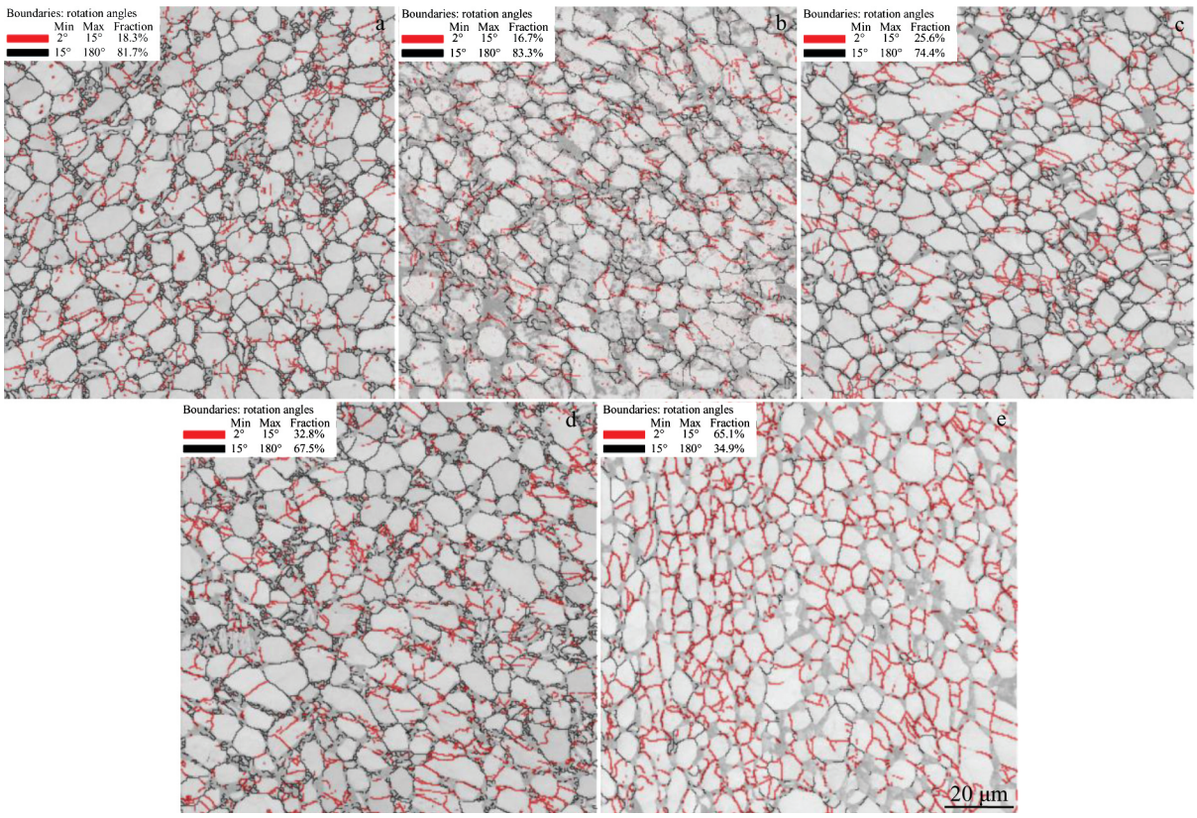

Fig.5 EBSD images of grain boundary orientation under different conditions: (a) original, (b) 500 °C/100 MPa, (c) 500 °C/300 MPa, (d) 600 °C/100 MPa, and (e) 600 °C/300 MPa

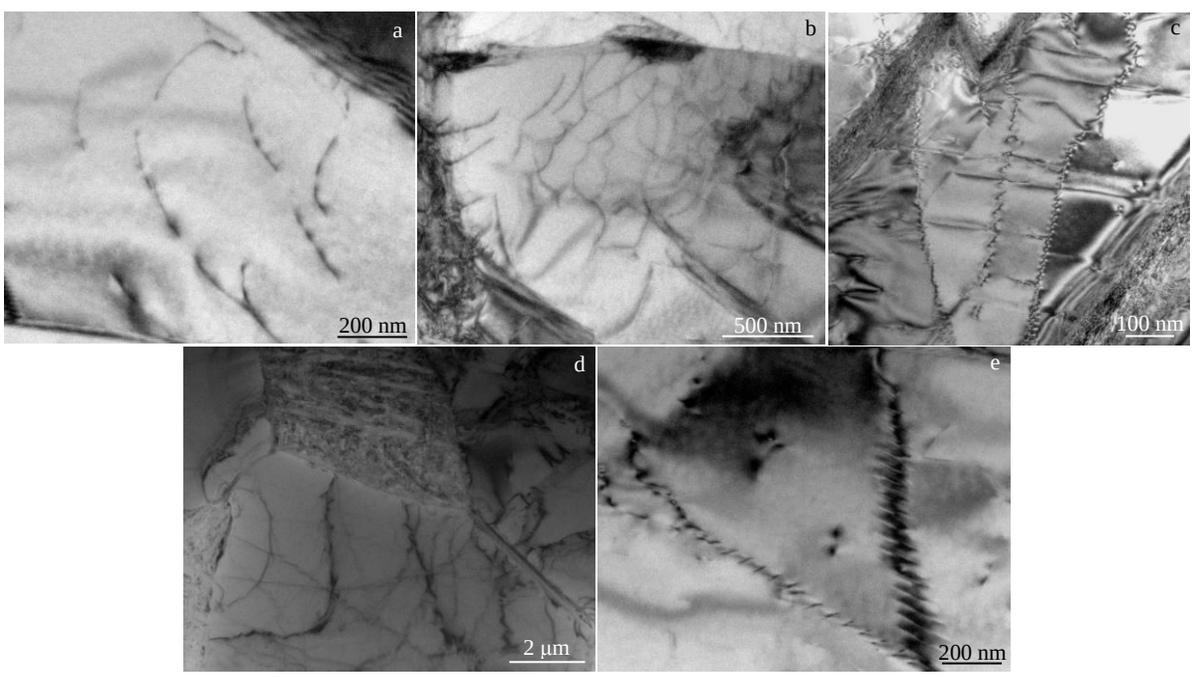

Fig.6 TEM images of specimens under different conditions: (a) original, (b) 500 °C/100 MPa, (c) 500 °C/300 MPa, (d) 600 °C/100 MPa, and (e) 600 °C/300 MPa

is greatly reduced. The impediment of the dislocation slip between α grains weakens. Meanwhile, more β phase enters the α grain boundary, as shown in Fig. 6, which further promotes the rotation of α grains. In this process, the stress

concentration can also be released. On the one hand, the high stress can produce a large number of dislocations; on the other hand, the dislocation slip leads to the decrease in stress. The dislocation entanglement results in the formation of dislocation cells and sub-grain boundaries. Thus, it is observed that many small grains are generated under initial stress of 300 MPa at 600 °C.

Fig.7 shows the distribution of grain size and aspect ratio in the specimen before and after stress relaxation. The average grain size D and aspect ratio R of α grain is calculated as 12.90 μm and 1.54 of original alloy, respectively. It can be seen that the original specimen is composed of nearly equiaxed grains, which is caused by dynamic recrystallization during forging. At 500 °C, the average grain size and aspect ratio are barely changed under initial stress of 100 MPa, compared with those of original alloy. The average aspect ratio is reduced under initial stress of 300 MPa at 500 °C, proving that some sub-grains appear during the recovery process and the sub-grain boundary is transformed into high angle grain boundary by the boundary migration. However, at 600 °C, some grains are coarsened with the size of 8 μm and increased under initial stress of 100 MPa. On the one hand, the vacancy is easily generated in tensile stress area and moves to compressive stress area. On the other hand, the high temperature may cause active diffusion and the boundary is easier to migrate. Therefore, the fine grains are increased obviously and some grains are lengthened under the initial stress of 300 MPa.

Fig. 8 shows the Schmid Factor (SF) distribution of {0001}<1010> slip system in α grains. The low SF means that the dislocation is difficult to move in some grains. SF mainly converges on 0.22~0.32 and 0.35~0.50 for the original alloy. After the stress relaxation at 500 °C, the distribution of SF hardly changes, which illustrates that the number of soft orientation increases. After the stress relaxation at 600 °C, the fraction of SF around 0.35 and 0.45 rises largely, which means that the dislocation is easier to move in some grains. Therefore, at 600 °C, the dislocation slip is the main mechanism of stress relaxation.

Fig.9 shows the {0001} pole diagrams of specimens under different conditions. The peak intensity I_{max} of the original specimen is 6.09, as shown in Fig. 6a. At 500 °C, the peak intensity decreases slightly to 5.56 after stress relaxation under initial stress of 100 MPa. When the initial stress increases to 300 MPa, the peak intensity is 9.07, indicating that the basal slip begins to play a role in stress relaxation process. At 600 °C, the peak intensity is 11.33 and 35.95 under 100 and 300 MPa, respectively. The dislocation slip becomes easier with increasing the stress relaxation temperature, which also implies that the dislocation slip gradually becomes the main mechanism of stress relaxation. It is worth noticing that the peak intensity of the specimen under initial stress of 300 MPa is far more than that of others. The formed strong texture indicates that the dislocation slip is no longer the main mechanism of stress relaxation. The grain rotation and grain boundary slip dominate the stress relaxation process in this case. Nevertheless, such strong texture may influence the performance of alloys.

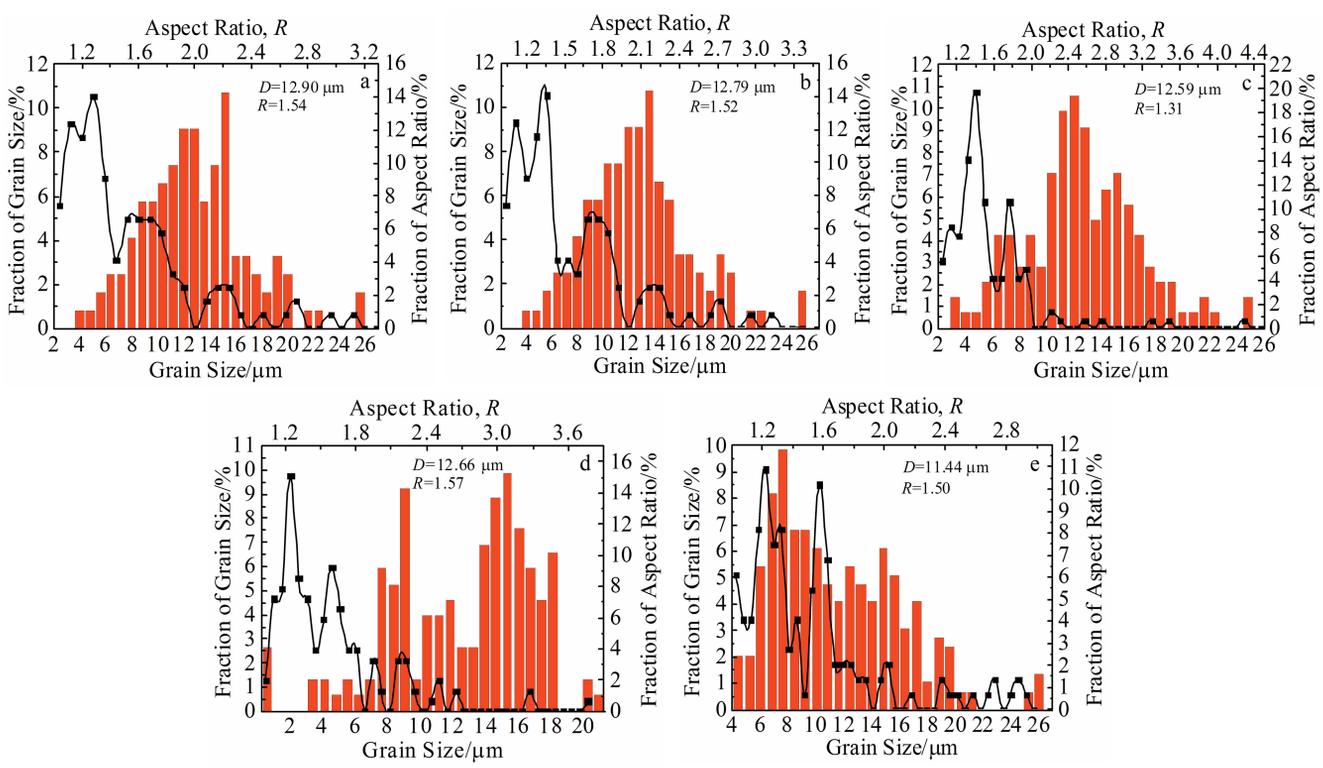

Fig.7 Grain size distribution and aspect ratio of specimens under different conditions: (a) original, (b) 500 °C/100 MPa, (c) 500 °C/300 MPa, (d) 600 °C/100 MPa, and (e) 600 °C/300 MPa

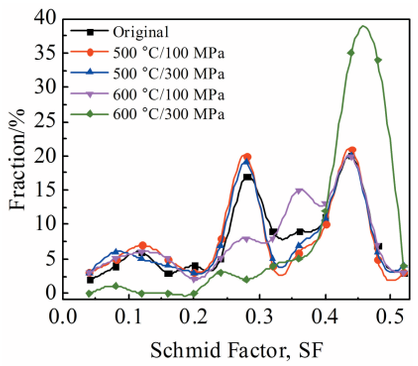

Fig.8 Schmid Factors of specimens under different conditions

2.3 Microstructure

As shown in Fig.10, the microstructure of titanium alloys is composed of primary α phase (α_p), secondary α phase (α_s), and β transformation structure (β_t). A fork-type structure appears on the end faces of the second α phase after stress relaxation, as indicated by the arrow in Fig. 10b, and it grows along the side of the second α phase, indicating that the fork-type structure is a β transition structure consisting of small secondary α phase and residual β phase. The appearance of the fork-type structure is mainly caused by the difference in the interface energy between the α phase and the β phase at different locations. The structure in α phase can separate the α lamellar phase along the width direction and thereby reduce the thickness of α lamellar phase. Because the thermal deformation parameters are the same, the thin α phase is easier to be equiaxed than the thick one. Therefore, the fork-type structure of the end face and the side face of the sheet α phase in titanium alloy provides favorable conditions for equiaxial process. Besides, it can be found from Fig.10 that the β phase is wedged into α/α interface as the Y shape with relatively high orientation difference, and the wedging of β phase occurs not only at the α/α interface of the crystal, but also at the α/α interface of the grain boundary. Thus, the wedging of β phase plays an important role in the equiaxial process of α phase. Due to the disordered arrangement of atoms at the grain boundary, the driving force of β/α phase transformation is rather large. Therefore, β/α transition can take place at the grain boundary firstly, which is consistent with the transformation from the lamellar α phases into β phases, as shown Fig. 10c and 10d. α phase can nucleate at several positions at the grain boundary simultaneously. As a result, the α phase of the grain boundary is spliced by a lot of α pieces, and the joints of the α phase become the preferred positions of β phase. It suggests that the wedging of β phase into the α/α interface plays an important role in the equiaxial process of both the grain boundary and the lamellar α phase.

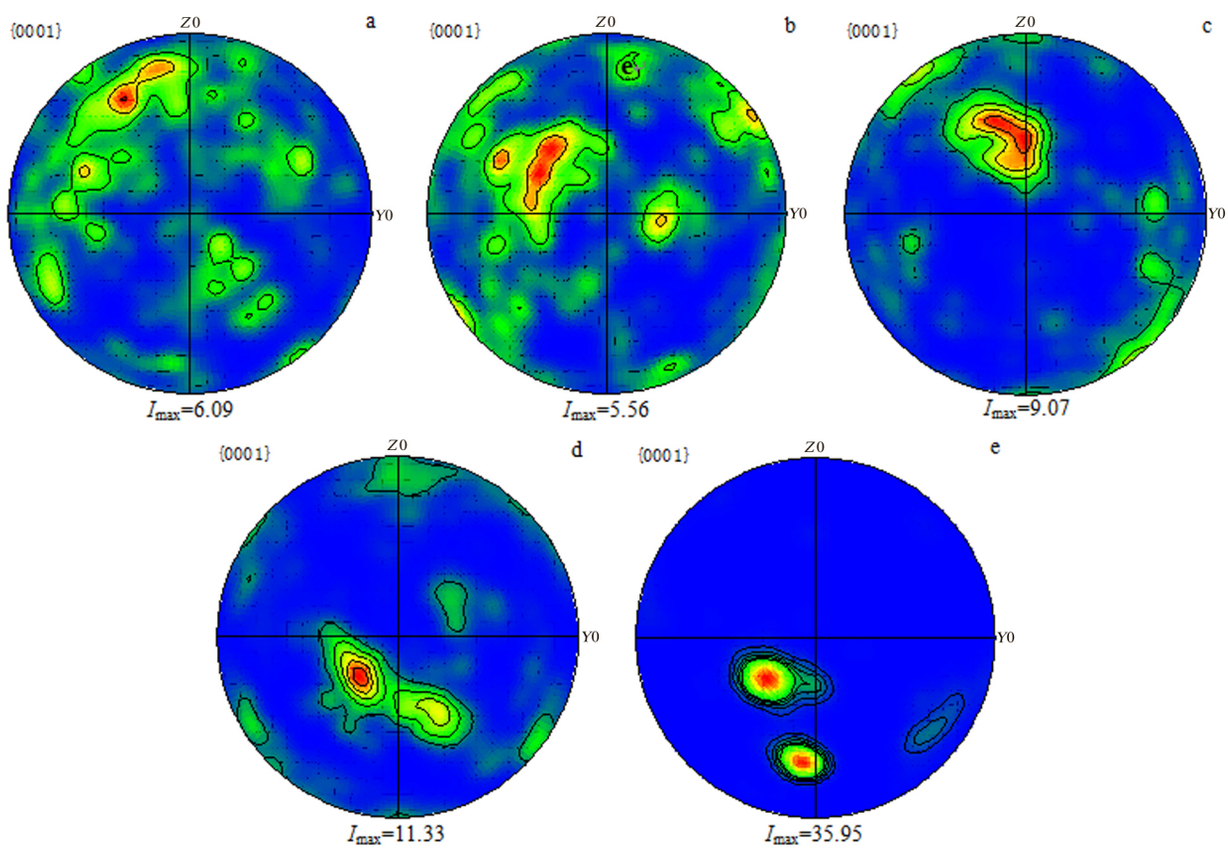

Fig.9 {0001} pole diagrams of specimens under different conditions: (a) original, (b) 500 °C/100 MPa, (c) 500 °C/300 MPa, (d) 600 °C/100 MPa, and (e) 600 °C/300 MPa

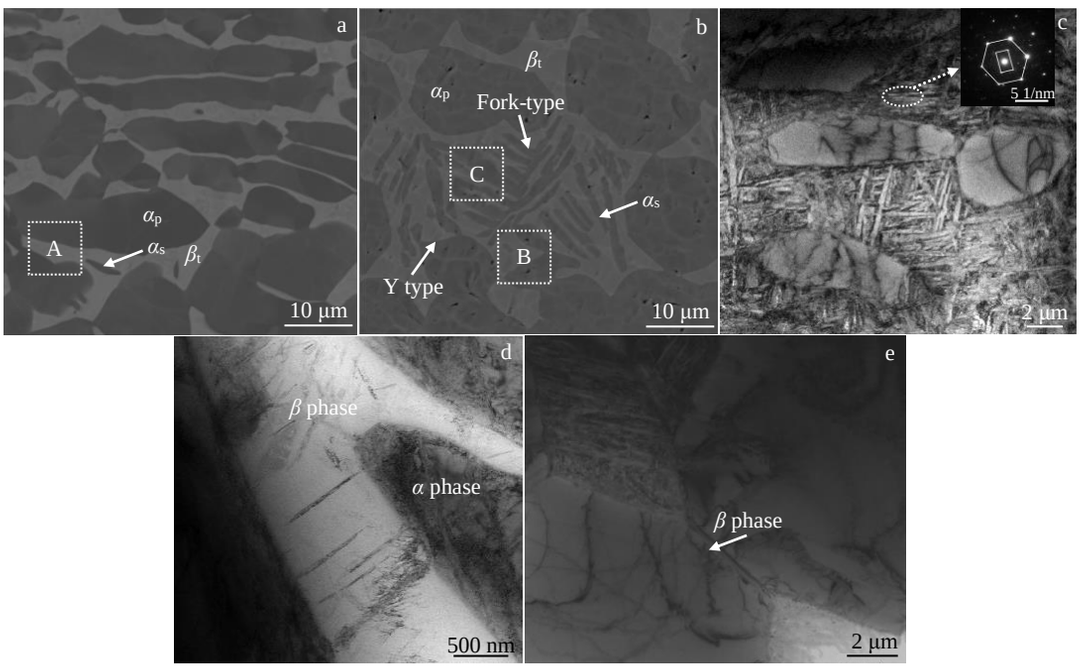

Fig.10 Microstructures of specimens under different conditions: (a) original, (b) 500 °C/100 MPa, (c) 500 °C/300 MPa, (d) 600 °C/100 MPa, and (e) 600 °C/300 MPa

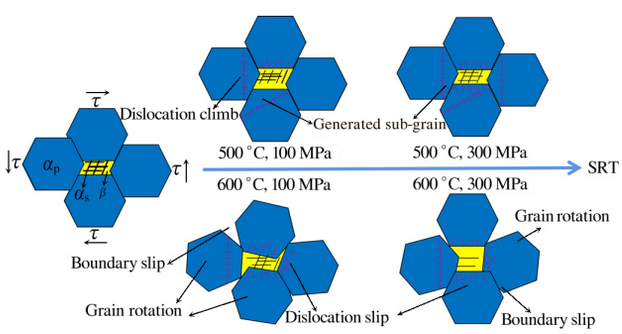

Fig.11 Schematic diagram of stress relaxation mechanism under different conditions

2.4 Stress relaxation mechanism

The main mechanism of stress relaxation is shown in Fig.11. At 500 °C, the dislocation slip is difficult to occur due to the α/β interface in specimens under initial stress of 100 MPa. However, the dislocation and phase interface provide many channels for fast diffusion. Thus, the dislocation climb is still easy to occur at low temperature. Meanwhile, a few sub-grains and sub-grain boundaries are generated. As the initial stress is increased to 300 MPa, there are more dislocation participating in dislocation slip. It is known that the slip of edge dislocation is faster than the climb of screw dislocation, resulting in the fact that the higher initial stress can reach SRL more quickly. At 600 °C, the grain boundary and phase interface change more actively, and a few grains begin to rotate under the initial stress of 100 MPa. Besides, β phase is softer than α phase. Thus, β phase is prone to producing larger deformation and promoting the grain rotation with simultaneous boundary slip. Consequently, the coarsening or lengthening of grains happens. However, the fraction of β phase increases quickly in β transformation structure under initial stress of 300 MPa, which further contributes to the α grain rotation and stress relaxation.

3 Conclusions

1) Higher temperature of 600 °C can release more stress during the heat treatment for Ti-6.5Al-2Zr-1Mo-1V alloy. However, the relaxation rate coefficient C_R is basically irrelevant with temperature under high initial stress. Thus, it is economical and effective that the higher stress is released at 500 °C and the lower stress is released at 600 °C during heat treatment.

2) The stress exponent is 2.38~7.76 under different temperatures and different initial stresses, which reflects different stress relaxation mechanisms.

3) The dislocation climb and recovery creep are the main stress relaxation mechanisms at 500 °C, and the dislocation slip also plays an important role in stress relaxation. With increasing the temperature, the dislocation slip basically controls the stress relaxation process. However, the stress relaxation mechanism is dominated by grain rotation and boundary slip at 600 °C.

4) The stress relaxation process has little impact on the structure of alloys after stress relaxation at 500 °C. However, the grain refinement becomes obvious under the initial stress of 300 MPa at 600 °C.

5) The increasing content of β phase contributes to the grain

refinement of α phase.

Reference

1 Chen Guoxing, Liu Caiyi. *Rare Metal Materials and Engineering* [J], 2020, 49(11): 3662

2 Vishnu J, Sankar M, Rack H J *et al*. *Materials Science and Engineering A*[J], 2020, 779: 139 127

3 Jiang Junjie, Ren Zhihao, Ma Zhibo *et al*. *Materials Science and Engineering A*[J], 2020, 772: 138 742

4 Boyer R R. *Materials Science and Engineering A*[J], 1996, 213(1-2): 103

5 Zhan Yu, Liu Chen, Zhang Junjian *et al*. *Materials Science and Engineering A*[J], 2019, 762: 138 093

6 Hrabe N, Gnäupel-Herold T, Quinn T. *International Journal of Fatigue*[J], 2017, 94: 202

7 Baragetti S, Arcieri E V. *Procedia Structural Integrity*[J], 2019, 24: 91

8 Meyers M A, Chawla K K. *Mechanical Behavior of Materials* [M]. Cambridge: Cambridge University Press, 2008

9 Dupeux M, Henriet J, Ignat M. *Acta Metall*[J], 1987, 35(9): 2203

10 Liu P, Zong Y, Shan D *et al*. *Materials Science and Engineering A*[J], 2015, 638: 106

11 Zong Yingying, Liu Po, Guo Bin *et al*. *Materials Science and Engineering A*[J], 2015, 620: 172

12 Luo Jingfeng, Xiong Wei, Li Xifeng. *Materials Science and Engineering A*[J], 2019, 743: 755

13 Zhu Kaiyuan, Li Zhiqiang, Fan Genlian *et al*. *Journal of Materials Research and Technology*[J], 2019, 8(2): 2201

14 Guo J Q, Zhang W, Sun X H. *Advanced Materials Research*[J], 2012, 455-456: 1434

15 Chandler H D. *Materials Science and Engineering A*[J], 2010, 527(23): 6219

16 Stone D, Wilson H, Kuo R C *et al*. *Scripta Metallurgica*[J], 1987, 21(11): 1559

17 Reif S K, Amberge K J, Woodford D A. *Materials & Design*[J], 1995, 16(1): 15

18 Guo J Q, Xuan F Z, Wang Z D *et al*. *Nuclear Power Engineering* [J], 2009, 30(4): 9

19 Boyer R R. *Materials Science Forum*[C]. Zurich-Uetikon: Trans Tech Publications Ltd, 2003, 426: 643

20 Zeng Yanping, Yao Dazhi, Cai Wenhe *et al*. *Rare Metal Materials and Engineering*[J], 2017, 46(11): 3316 (in Chinese)

Ti-6.5Al-2Zr-1Mo-1V钛合金低温应力松弛及组织演变

黄　镇，袁武华，朱佳佳

(湖南大学 材料科学与工程学院，湖南 长沙 410082)

摘　要：在500、550和600 ℃及不同初始应力下对Ti-6.5Al-2Zr-1Mo-1V钛合金进行了应力松弛实验。基于经典的Maxwell指数衰减函数，得到了应力松弛极限。提出了利用松弛稳定系数（C_S）和松弛速率系数（C_R）来描述Ti-6.5Al-2Zr-1Mo-1V合金的松弛特性，有利于制定残余应力消减工艺。根据Norton和Arrhenius方程计算了应力指数。通过应力指数和显微组织分析，阐明了应力松弛机理。在不同初始应力下，500 ℃时，位错的攀移和扩散主导了应力松弛过程；550 ℃时，位错滑移在应力松弛过程中起主要作用；600 ℃时，位错滑移、边界滑移和晶粒旋转控制着松弛过程。

关键词：钛合金；应力松弛；微观组织；松弛机制

作者简介：黄　镇，男，1996年生，硕士生，湖南大学材料科学与工程学院，湖南 长沙 410082，E-mail：862750540@qq.com